Investigo
Universidade de Vigo

Biblioteca Universitaria
Área de Repositorio Institucional

Tfno.: 986 813 821
investigo@uvigo.gal

Accepted version.

Citation for published version:

Yu, J., Menviel, L., Jin, Z.D. et al. Last glacial atmospheric CO2 decline due to widespread Pacific deep-water expansion. Nat. Geosci. 13, 628–633 (2020).
https://doi.org/10.1038/s41561-020-0610-5

This version of the article has been accepted for publication, after peer review and is subject to Springer Nature’s AM terms of use but is not the Version of Record and does not reflect post-acceptance improvements, or any corrections. The Version of Record is available online at https://doi.org/10.1038/s41561-020-0610-5

General rights:

Copyright © 2020, The Author(s), under exclusive license to Springer Nature Limited

Last glacial atmospheric CO_2 decline due to widespread Pacific deep water expansion

J. Yu[1,2]*, L. Menviel[3], Z.D. Jin[2,4,5], R.F. Anderson[6], Z. Jian[7], A.M. Piotrowski[8], X. Ma[2], E.J. Rohling[1,9], F. Zhang[2,4], G. Marino[1,10], J.F. McManus[6]

[1]Research School of Earth Sciences, The Australian National University, Canberra, ACT 2601, Australia.

[2]State Key Laboratory of Loess and Quaternary Geology, Institute of Earth Environment, Chinese Academy of Sciences, Xi'an 710075, China.

[3]Climate Change Research Centre, University of New South Wales, Sydney, NSW 2052, Australia.

[4]CAS Center for Excellence in Quaternary Science and Global Change, Xi'an, 710061, China.

[5]Open Studio for Oceanic-Continental Climate and Environment Changes, Qingdao National Laboratory for Marine Science and Technology, Qingdao, 266061, China.

[6]Lamont-Doherty Earth Observatory, Columbia University, New York, New York, 10964, USA.

[7]State Key Laboratory of Marine Geology, Tongji University, Shanghai, 200092, China.

[8]Department of Earth Sciences, University of Cambridge, Cambridge, CB2 3EQ, UK.

[9]Ocean and Earth Science, University of Southampton, National Oceanography Centre, Southampton SO14 3ZH, UK.

[10]Department of Marine Geosciences and Territorial Planning and CIM-UVIGO, University of Vigo, 36310 Vigo, Spain.

*Correspondence to: jimin.yu@anu.edu.au

Ocean circulation critical affects global climate and atmospheric CO_2 through redistributing heat and carbon in the Earth system. Despite intensive research, the nature of past ocean circulation changes remains elusive. Here we present deep-water carbonate ion concentration ($[CO_3^{2-}]$; low values indicating carbon-rich waters) reconstructions for widely distributed locations in the Atlantic Ocean, and these data show a low-$[CO_3^{2-}]$ water mass that extended northward up to about 20°S in the South Atlantic at 3-4 km depth during the Last Glacial Maximum. In combination with radiocarbon ages, neodymium isotopes and carbon isotopes, we conclude that this low-$[CO_3^{2-}]$ signal reflects a widespread expansion of carbon-rich Pacific deep waters into the South Atlantic, revealing a glacial deep Atlantic circulation scheme different than commonly considered. Comparison of high-resolution $[CO_3^{2-}]$ records from different water depths in the South Atlantic indicates that this expansion developed from approximately 38 to 28 thousand years ago. We infer that its associated carbon sequestration may have contributed critically to the contemporaneous atmospheric CO_2 decline, thereby helping to initiate the glacial maximum.

Ocean circulation and the carbon cycle are intricately linked, and ocean circulation reconstructions can therefore provide important insights into mechanisms of past atmospheric CO_2 changes. Circulation in the deep Atlantic (>~2.5 km) during the Last Glacial Maximum (LGM; 18-22 ka) is traditionally viewed as following a mixing model between deep waters formed in the basin's polar regions, without much contribution of waters from other oceans[1-4]. Using this long-held ocean circulation model, however, it is difficult to explain the observed older radiocarbon (^{14}C) ages and more radiogenic neodymium isotopic (εNd) signatures at ~3.8 km than at ~5 km in the LGM South Atlantic[5,6] (Fig. 1). Burke et al.[7] showed that sluggish recirculation of southern-sourced waters combined with reduced mixing with ^{14}C-rich northern-sourced waters can contribute to old ^{14}C ages at ~3.8 km, in the absence of interocean water-mass interactions. Yet, additional mechanisms are likely needed to fully explain the depth structure and large magnitude of ^{14}C-age changes, along with the more radiogenic εNd signal observed at 3.8 km (Fig. 1). Pacific deep waters (PDW) can significantly affect deglacial εNd signatures in Drake Passage (Southern Ocean)[8], but its role in the deep South Atlantic during the LGM remains unexplored. PDW stores a large amount of respired carbon[9,10], and thus temporal changes in its volumetric extent would have important implications for past atmospheric CO_2 levels.

Deep-water carbonate ion concentrations ($[CO_3^{2-}]$) can provide critical information about past deep ocean circulation and dissolved inorganic carbon (DIC) changes. In the modern Atlantic, contrasting $[CO_3^{2-}]$ signatures between water masses reflect ocean circulation patterns[11] (Fig. 2). Also, past DIC changes may be quantified from $[CO_3^{2-}]$ reconstructions[12]. Here, we present deep-water $[CO_3^{2-}]$ reconstructions for extensive locations in the Atlantic to decipher the role of ocean circulation in the glacial atmospheric CO_2 decrease. We focus on deep South Atlantic hydrography, which remains incompletely understood despite intensive studies[5-8,13-16].

First meridional $[CO_3^{2-}]$ transect for the LGM Atlantic

We have reconstructed deep-water $[CO_3^{2-}]$ using benthic B/Ca for the Holocene (0-5 ka) and LGM samples from 41 cores (Fig. 2; Supplementary Fig. 1-3). Five cores at 3-4.2 km and an abyssal core at ~5 km from the South Atlantic were chosen to investigate reasons for ^{14}C and εNd anomalies at 3.8 km water depth (Fig. 1, 2a). Thirty additional cores from widely spread locations

(1.1-4.7 km, 36°S-62°N) in the Atlantic and five cores at 3-4 km from the equatorial Pacific provide a broader context of water-mass signatures. Benthic B/Ca is converted into deep-water [CO_3^{2-}] using species-specific global core-top calibrations[17]. The uncertainty associated with [CO_3^{2-}] reconstructions is ~5 μmol/kg (ref. [17]). Detailed information about samples and analytical methods along with new (n = 173 samples) and compiled (n = 260 samples) data is given in Methods and Supplementary Tables 1-11.

Fig. 2c shows the first meridional [CO_3^{2-}] transect for the deep Atlantic during the LGM (Methods). Given the locations of studied cores, this transect mainly reflects [CO_3^{2-}] distributions for eastern Atlantic basins. Future work is needed to investigate the extent of zonal homogeneity in the LGM Atlantic. Above ~2.5 km, [CO_3^{2-}] of glacial North Atlantic waters reached up to ~140 μmol/kg, which is ~20 μmol/kg higher than in modern North Atlantic Deep Water (NADW)[11]. These waters likely represent the previously documented well-ventilated Glacial North Atlantic Intermediate Waters (GNAIW)[1,2,18-20]. Below ~2.5 km, LGM North Atlantic [CO_3^{2-}] values were up to ~20 μmol/kg lower than today, consistent with greater mixing/advection of low-[CO_3^{2-}] Glacial Antarctic Bottom Waters (GAABW) and/or increased biological respiration in the glacial ocean[1,2,19,21-23]. The boundary between LGM upper and lower water masses at ~2.5 km is consistent with reconstructions from other proxies ($\delta^{13}C$, Cd/Ca, and εNd) and modeling[1-3,19,24,25].

In the South Atlantic, deep-water [CO_3^{2-}] in the 5 studied cores from ~3-4 km water depth are lower by ~20 μmol/kg during the LGM than the Holocene, consistent with the sign of change from qualitative [CO_3^{2-}] proxies from the same cores[26-28] (Supplementary Fig. 2). By contrast, opposite LGM-Holocene [CO_3^{2-}] changes are observed in abyssal core TNO57-21 (41.1°S, 7.8°E, 4981 m). TNO57-21 shows slightly higher abyssal [CO_3^{2-}] during the LGM than the Holocene, supported by multiple benthic B/Ca measurements in this core and qualitative proxies (%$CaCO_3$ and foraminiferal fragmentation) for several South Atlantic cores at similar depths[15,26,27] (Supplementary Fig. 3). Our data reveal that a low-[CO_3^{2-}] (<80 μmol/kg) water mass, centered at ~3.5 km and extending northward up to ~20°S, overlay a relatively high-[CO_3^{2-}] (>80 μmol/kg) abyssal water mass in the LGM South Atlantic (Fig. 2c).

Circulation and biological influences within the Atlantic

Below, we discuss the nature of our newly discovered low-[CO_3^{2-}] deep South Atlantic water mass (Fig. 2). Deep-water [CO_3^{2-}] is affected by changes in endmember values, biological respiration, and water-mass mixing. We combine [CO_3^{2-}] with benthic $\delta^{13}C$ and εNd to investigate influences from these processes (Fig. 3). To provide a context, we start with the Holocene data. Modern water-mass endmember values are assigned following the literature[1,3,23]. As shown in Fig. 3a-b, Holocene deep-water signatures at the studied cores, including the 5 cores at ~3-4 km from the South Atlantic, fall along the NADW-AABW mixing trends, consistent with the established knowledge[1-3,19].

For the LGM, we first investigate water-mass endmember changes (Fig. 3c, d). To do so, we identify sites with benthic $\delta^{13}C$ values similar to the $\delta^{13}C$ endmembers defined by refs [1-3,19]. Deep-water [CO_3^{2-}] reconstructions for these sites are then chosen as corresponding [CO_3^{2-}] water-mass endmembers. Thus, we choose $\delta^{13}C$ = ~1.5‰ and [CO_3^{2-}] = ~140 μmol/kg as endmember values for GNAIW, and $\delta^{13}C$ = ~-0.8‰ and [CO_3^{2-}] = ~85 μmol/kg for GAABW (Supplementary Table 3). The εNd endmember for GNAIW is debated[3,29], and we assign a range of values of ~-

13.5 to ~-10.5 to this water mass. Using other εNd values for GNAIW would have little influence on our conclusions, as long as GNAIW had less radiogenic εNd than GAABW. For GAABW, we choose LGM εNd measurements (~-6.7) from TNO57-21[6], the same site used to pin down $\delta^{13}C$ and $[CO_3^{2-}]$ endmember values[1]. Our choice is different from ref. [3], which used LGM measurements from MD07-3076Q to characterize GAABW εNd. Compared to TNO57-21 (5 km), MD07-3076Q (44.2°S, 14.2°W, 3770 m) is located at a much shallower water depth near the mid-ocean ridge, and was bathed in warmer and less saline deep waters during the LGM[30]. By contrast, core TNO57-21 was retrieved from the abyssal Cape Basin, and is ideally located downstream of AABW formed on Antarctic shelves. Previous pore-water reconstructions suggest extremely cold and saline waters in the abyssal Cape Basin during the LGM[16], lending strong support to using TNO57-21 for determining GAABW endmember values.

Given the above endmember values, it is impossible to explain the low-$[CO_3^{2-}]$ water mass signature at ~3-4 km in the LGM South Atlantic by conservative mixing between GNAIW and GAABW, because this water mass had even lower $[CO_3^{2-}]$ values than GAABW (Fig. 2, 3). Previous work[7,31,32] proposed sluggish GAABW recirculation in the lower cell (>~2.5 km) of the Atlantic during the LGM. In this case, the South Atlantic low-$[CO_3^{2-}]$ signature at ~3-4 km might be viewed as a consequence of respired carbon accumulation due to water mass aging, analogous to the cause of today's low-$[CO_3^{2-}]$ signature of PDW[11,33] (Supplementary Fig. 4). Respiration would decrease $\delta^{13}C$ and $[CO_3^{2-}]$ along the Redfield slope, with little impact on εNd[3,23]. Were the low-$[CO_3^{2-}]$ in the five South Atlantic cores due to enhanced respiration effects, then the combined $[CO_3^{2-}]$ and $\delta^{13}C$ values would imply an almost pure GNAIW source water (Fig. 3c). However, this is contradicted by much more radiogenic εNd values (-5 to -9) than those of GNAIW (~-13.5

to ~-10.5) (Fig. 3d). Therefore, the low-[CO_3^{2-}] signature of the LGM South Atlantic water mass at 3-4 km cannot be explained by a combination of mixing and respiration that involves only GNAIW and GAABW.

Glacial Pacific deep water expansion into the Atlantic

Considering that deep waters from the Pacific generally have high-DIC and low-[CO_3^{2-}] values[9,11,18], we explore whether the low-[CO_3^{2-}] water mass recorded by the 5 South Atlantic cores was affected by Glacial Pacific Deep Waters (GPDW). The GPDW endmember $\delta^{13}C$ and εNd values are set to -0.4‰ and -3.5, respectively[34-36] (Fig. 3; Supplementary Table 3). Currently, there are no benthic B/Ca data to define the GPDW [CO_3^{2-}] endmember because of intensive dissolution and scarce occurrence of the required species (see Methods) in the deep North Pacific. Nevertheless, foraminiferal assemblage and boron isotope (based on mixed species of genus *Cibicidoides*) data[37,38] suggest similar [CO_3^{2-}] values between the Holocene and the LGM in this region. Therefore, we assume that GPDW had the same endmember [CO_3^{2-}] (~50 μmol/kg) as modern PDW. We acknowledge potential uncertainties with this endmember, but our main conclusion requires only that GPDW had lower [CO_3^{2-}] GAABW, which is supported by published data[18,39-42]. Located downstream of GPDW, all examined cores at 3-4 km from the equatorial Pacific show lower LGM [CO_3^{2-}] (61-76 μmol/kg) than GAABW (>80 μmol/kg) (Fig. 3c). In the modern ocean, PDW [CO_3^{2-}] increases during its southward transport due to mixing with younger, lower-DIC waters (Supplementary Fig. 4). Benthic $\delta^{13}C$ mapping[34] indicates that the basic ocean circulation pattern seen today operated in the LGM Pacific. Therefore, GPDW likely had a lower [CO_3^{2-}] than GAABW, a situation also expected from much older ages and likely more respired carbon contents in GPDW[38,43].

In $[CO_3^{2-}]$-$\delta^{13}C$ space, data from the five South Atlantic cores suggest a mixing scheme involving three water masses: GNAIW, GAABW, and GPDW (Fig. 3c). Deep-water $[CO_3^{2-}]$ and εNd values at these locations can be explained by mixing GPDW with aged GNAIW-GAABW mixtures (Fig. 3d), although insufficient knowledge of endmember εNd and Nd contents preclude exact quantification of mixing and respiration effects (Supplementary Fig. 5, 6). Paired $[CO_3^{2-}]$-^{14}C age data are too limited to allow a detailed investigation, but mixing of GPDW into the LGM South Atlantic is qualitatively consistent with the very old ventilation age at MD07-3076Q (Fig. 1)[5]. Therefore, we attribute the low $[CO_3^{2-}]$ values at 3-4 km in the LGM South Atlantic to the admixture of low-$[CO_3^{2-}]$ GPDW. The presence of low-$[CO_3^{2-}]$ deep-water as far north as ~20°S in the South Atlantic suggests a substantial expansion of GPDW during the LGM (Fig. 2c). This is different from the long-held view that largely focuses on changes in water masses formed solely within the glacial Atlantic.

Prevailing evidence suggests a sluggish circulation, characterized by reduced water-mass mixing in the LGM Pacific Ocean[24,25,34]. This would allow southward expansion of the recirculated GPDW and better preservation of its low-$[CO_3^{2-}]$, more-radiogenic-εNd, and old-^{14}C age signatures during transport. This is supported by findings of a "floating" high-DIC, low-$[CO_3^{2-}]$, and very old deep water in the equatorial and South Pacific during the LGM[18,44]. Entrainment into the Antarctic Circumpolar Current at the latitude of Drake Passage (~60°S) would have facilitated GPDW transport into the South Atlantic[33], analogous to what happens today albeit with greater GPDW influences in the LGM Southern Ocean (Supplementary Fig. 7). In contrast to vigorous and deep southward NADW transport today, shoaled GNAIW formation would allow greater northward expansion of GPDW in the deep (>~2.5 km) Atlantic at the LGM (Fig. 2). Owing to inevitable mixing with surrounding waters during transport, we use the term modified GPDW (mGPDW) in Fig. 2c.

It's worth noting that our proposed GPDW expansion does not necessarily exclude deep-water recirculation within the LGM Atlantic, as suggested previously[7]. Both processes may be needed to fully explain proxy data in the LGM ocean. We also note that while GAABW $\delta^{13}C$ is a matter of long-standing debate[45], alternative scenarios to define this endmember do not affect our conclusions (Supplementary Fig. 8).

Timing of GPDW expansion and atmospheric CO_2 decline

To determine the timing of GPDW expansion, we have extended the previously published [CO_3^{2-}] record (0-27 ka)[42] to 60 ka for core TNO57-21 (downstream of GAABW), and then compared it with a published [CO_3^{2-}] record for core MD07-3076Q[28], which is located close to the core of the low-[CO_3^{2-}] water mass (Fig. 2, 4). Prior to ~38 ka, the long-term deep-water [CO_3^{2-}] at 3.8 km (MD07-3076Q) was slightly higher than at 5 km (TNO57-21), similar to the modern bathymetric [CO_3^{2-}] distribution in the South Atlantic[11] (Fig. 2a). From ~38 to ~28 ka, a reversal of the vertical [CO_3^{2-}] gradient developed between the two depths, coeval with a significant aging of deep waters at MD07-3076Q[46]. We suggest that the development of this [CO_3^{2-}] gradient reversal reflects sizable GPDW expansion. This reversal broadly corresponded to the maximum advance of the Antarctic ice sheet, possibly associated with a GAABW weakening[24]. If so, reduced GAABW production might have facilitated the development of the low-[CO_3^{2-}] anomaly at 3-4 km in the South Atlantic. Over the entire duration of the LGM, deep-water [CO_3^{2-}] at 3.8 km was persistently ~15 µmol/kg lower than at 5 km, suggesting full establishment of low-[CO_3^{2-}] GPDW expansion in the South Atlantic (Fig. 2). Superimposed on the long-term changes, we find that deep-water [CO_3^{2-}] converged between MD07-3076 and TNO57-21 during Heinrich Stadials, consistent with previously reconstructed erosion of chemical gradients in the deep Southern Ocean due to enhanced vertical mixing[46,47]. Overall, the large and reversed [CO_3^{2-}] gradient between MD07-3076Q and TNO57-21 lends strong observational support to the role of sluggish ocean circulation in sequestering carbon during the LGM[24,25].

Our deep-water [CO_3^{2-}] reconstructions offer a means to quantify carbon storage changes in the past. Below 3 km water depth, Atlantic [CO_3^{2-}] was ~15 µmol/kg lower on average during the LGM relative to the Holocene (Fig. 2; Supplementary Table 4). Based on the relationship from ref. [12], this suggests at least ~25 µmol/kg increase in DIC. Using a mass of 10×10^{19} kg for waters below 3 km in the Atlantic, this implies that the deep Atlantic sequestered ~30 Gigatonnes extra carbon during the LGM relative to the Holocene. But, this estimate likely represents a lower limit of carbon sequestration. If our inferred GPDW expansion is correct, then it would imply extensive occupation of low-[CO_3^{2-}] and high-DIC deep waters in the voluminous Indo-Pacific oceans. Respired carbon contents are high in the deep Pacific today, and may have been even higher during the LGM, as suggested by reduced glacial deep-sea O_2 levels[9,10,48]. By sequestering more respired carbon and nutrient in the ocean interior, GPDW expansion would have decreased the preformed nutrient levels[10], enhanced the global biological pump efficiency, and thus contributed to lowering atmospheric CO_2. Given coeval low-[CO_3^{2-}] water mass formation and the ~20 ppm atmospheric CO_2 drop[49] (Fig. 4), we suggest that expansion of high-DIC GPDW was a key contributor to the final atmospheric CO_2 drawdown and thereby helped push the global climate into glacial maximum conditions.

References

1. Oppo D, Gebbie G, Huang KF, Curry W, Marchitto T, Pietro KR. Data Constraints on Glacial Atlantic Water Mass Geometry and Properties. *Paleoceanography and Paleoclimatology* 2018, **33**(9)**:** 1013-1034.

2. Lynch-Stieglitz J, Adkins JF, Curry WB, Dokken T, Hall IR, Herguera JC*, et al.* Atlantic meridional overturning circulation during the Last Glacial Maximum. *Science* 2007, **316**(5821)**:** 66-69.

3. Howe JNW, Piotrowski A, Noble TL, Mulitza S, Chiessi CM, Bayon G. North Atlantic Deep Water Production during the Last Glacial Maximum. *Nat Commun* 2016, **7:** doi: 10.1038/ncomms11765.

4. Gebbie G. How much did Glacial North AtlanticWater shoal? *Paleoceanogr* 2014, **29**(3)**:** 190-209.

5. Skinner L, Fallon SJ, Waelbroeck C, Michel E, Barker S. Ventilation of the Deep Southern Ocean and Deglacial CO_2 Rise. *Science* 2010, **328:** 1147-1151.

6. Piotrowski A, Galy A, Nicholl JAL, Roberts N, Wilson DJ, Clegg JA*, et al.* Reconstructing deglacial North and South Atlantic deep water sourcing using foraminiferal Nd isotopes. *Earth Planet Sci Lett* 2012, **357-358:** 289-297.

7. Burke A, Stewart AL, Adkins JF, Ferrari R, Jansen MF, Thompson AF. The glacial mid-depth radiocarbon bulge and its implications for the overturning circulation. *Paleoceanogr* 2015, **30**(7)**:** 1021-1039.

8. Robinson LF, van de Flierdt T. Southern Ocean evidence for reduced export of North Atlantic Deep Water during Heinrich event 1. *Geology* 2009, **37:** 195-198.

9. Anderson RF, Sachs JP, Fleisher MQ, Allen KA, Yu J, Koutavas A*, et al.* Deep-sea oxygen depletion and ocean carbon sequestration during the last ice age. *Glob Biogeochem Cycle* 2019, **33**(3)**:** doi:10.1029/2018GB006049.

10. Jaccard SL, Galbraith ED. Large climate-driven changes of oceanic oxygen concentrations during the last deglaciation. *Nature Geoscience* 2012, **5**(2)**:** 151-156.

11. Key RM, Kozyr A, Sabine CL, Lee K, Wanninkhof R, Bullister JL*, et al.* A global ocean carbon climatology: Results from Global Data Analysis Project (GLODAP). *Glob Biogeochem Cycle* 2004, **18**(4)**:** doi: 10.1029/2004GB002247.

12. Yu J, Menviel L, Jin ZD, Thornalley DJR, Barker S, Marino G*, et al.* Sequestration of carbon in the deep Atlantic during the last glaciation. *Nature Geoscience* 2016, **9**(4)**:** 319-324.

13. Burke A, Robinson LF. The Southern Ocean's role in carbon exchange during the last deglaciation. *Science* 2012, **335:** 557-561. doi:510.1126/science.1208163.

14. Skinner LC, Scrivner AE, Vance D, Barker S, Fallon S, Waelbroeck C. North Atlantic versus Southern Ocean contributions to a deglacial surge in deep ocean ventilation. *Geology* 2013, **41**(6)**:** 667-670.

15. Barker S, Knorr G, Vautravers M, Diz P, Skinner L. Extreme deepening of the Atlantic overturning circulation during deglaciation. *Nature Geoscience* 2010, **3:** 567-571.

16. Adkins JF, McIntyre K, Schrag DP. The salinity, temperature, and $\delta^{18}O$ of the glacial deep ocean. *Science* 2002, **298**(5599)**:** 1769-1773.

17. Yu JM, Elderfield H. Benthic foraminiferal B/Ca ratios reflect deep water carbonate saturation state. *Earth Planet Sci Lett* 2007, **258**(1-2)**:** 73-86, doi: 10.1016/j.epsl.2007.1003.1025.

18. Yu J, Broecker W, Elderfield H, Jin ZD, McManus J, Zhang F. Loss of carbon from the deep sea since the Last Glacial Maximum. *Science* 2010, **330:** 1084-1087, doi: 1010.1126/science.1193221.

19. Marchitto T, Broecker W. Deep water mass geometry in the glacial Atlantic Ocean: A review of constraints from the paleonutrient proxy Cd/Ca. *Geochem Geophys Geosyst* 2006, **7**(12)**:** doi:10.1029/2006GC001323.

20. Yu J, Menviel L, Jin ZD, Thornalley DJR, Foster GL, Rohling EJ*, et al.* More efficient North Atlantic carbon pump during the Last Glacial Maximum. *Nat Commun* 2019, **10:** ARTN 2170, 2110.1038/s41467-41019-10028-z.

21. Chalk TB, Foster GL, Wilson PA. Dynamic storage of glacial CO2 in the Atlantic Ocean revealed by boron [CO32−] and pH records. *Earth Planet Sci Lett* 2019, **510:** 1-11.

22. Broecker W, Yu J, Putnam AE. Two contributors to the glacial CO_2 decline. *Earth Planet Sci Lett* 2015**:** http://dx.doi.org/10.1016/j.epsl.2015.1007.1019.

23. Yu JM, Elderfield H, Piotrowski A. Seawater carbonate ion-$\delta^{13}C$ systematics and application to glacial-interglacial North Atlantic ocean circulation. *Earth Planet Sci Lett* 2008, **271**(1-4)**:** 209-220. doi:210.1016/j.epsl.2008.1004.1010.

24. Menviel L, Yu J, Joos F, Mouchet A, Meissner KJ, England MH. Poorly ventilated deep ocean at the Last Glacial Maximum inferred from carbon isotopes: A data-model comparison study. *Paleoceanogr* 2017, **31:** doi:10.1002/2016PA003024.

25. Muglia J, Skinner L, Schmittner A. Weak overturning circulation and high Southern Ocean nutrient utilization maximized glacial ocean carbon. *Earth Planet Sci Lett* 2018, **496:** 47-56.

26. Hodell DA, Charles CD, Sierro FJ. Late Pleistocene evolution of the ocean's carbonate system. *Earth Planet Sci Lett* 2001, **192**(2)**:** 109-124.

27. Gottschalk J, Hodell DA, Skinner LC, Crowhurst SJ, Jaccard SL, Charles C. Past Carbonate Preservation Events in the Deep Southeast Atlantic Ocean (Cape Basin) and Their Implications for Atlantic Overturning Dynamics and Marine Carbon Cycling. *Paleoceanography and Paleoclimatology* 2018, **33**(6)**:** 643-663.

28. Gottschalk J, Skinner LC, Misra S, Waelbroeck C, Menviel L, Timmermann A. Abrupt changes in the southern extent of North Atlantic Deep Water during Dansgaard-Oeschger events. *Nature Geoscience* 2015, **8**(12)**:** 950-U986.

29. Zhao N, Oppo DW, Huang K-F, Howe JNW, Blusztajn J, Keigwin LD. Glacial–interglacial Nd isotope variability of North Atlantic Deep Water modulated by North American ice sheet. *Nat Commun* 2019, **10**(1)**:** 5773.

30. Roberts J, Gottschalk J, Skinner LC, Peck VL, Kender S, Elderfield H*, et al.* Evolution of South Atlantic density and chemical stratification across the last deglaciation. *Proceedings of the National Academy of Sciences* 2016, **113**(3)**:** 514-519.

31. Ferrari R, Jansen MF, Adkins JF, Burke A, Stewart AL, Thompson AF. Antarctic sea ice control on ocean circulation in present and glacial climates. *P Natl Acad Sci USA* 2014, **111**(24)**:** 8753-8758.

32. Adkins JF. The role of deep ocean circulation in setting glacial climates. *Paleoceanogr* 2013, **28**(3)**:** 539-561.

33. Talley LD. Closure of the Global Overturning Circulation Through the Indian, Pacific, and Southern Oceans: Schematics and Transports. *Oceanography* 2013, **26**(1)**:** 80-97.

34. Matsumoto K, Oba T, Lynch-Stieglitz J, Yamamoto H. Interior hydrography and circulation of the glacial Pacific Ocean. *Quat Sci Rev* 2002, **21:** 1693-1704.

35. Hu R, Piotrowski AM, Bostock HC, Crowhurst S, Rennie V. Variability of neodymium isotopes associated with planktonic foraminifera in the Pacific Ocean during the Holocene and Last Glacial Maximum. *Earth Planet Sci Lett* 2016, **447:** 130-138.

36. Keigwin LD. North Pacific deep water formation during the latest glaciation. *Nature* 1987, **330**(6146)**:** 362-364.

37. Anderson DM, Archer D. Glacial-interglacial stability of ocean pH inferred from foraminifer dissolution rates. *Nature* 2002, **416**(6876)**:** 70-73.

38. Rae JWB, Sarnthein M, Foster GL, Ridgwell A, Grootes PM, Elliott T. Deep water formation in the North Pacific and deglacial CO_2 rise. *Paleoceanogr* 2014, **29**(6)**:** 645-667.

39. Umling NE, Thunell RC. Mid-depth respired carbon storage and oxygenation of the eastern equatorial Pacific over the last 25,000 years. *Quat Sci Rev* 2018, **189:** 43-56.

40. Doss W, Marchitto TM. Glacial deep ocean sequestration of CO_2 driven by the eastern equatorial Pacific biologic pump. *Earth Planet Sci Lett* 2013, **377:** 43-54.

41. Kerr J, Rickaby R, Yu JM, Elderfield H, Sadekov AY. The effect of ocean alkalinity and carbon transfer on deep-sea carbonate ion concentration during the past five glacial cycles. *Earth Planet Sci Lett* 2017, **471:** 42-53.

42. Yu J, Anderson RF, Jin ZD, Menviel L, Zhang F, Ryerson FJ*, et al.* Deep South Atlantic carbonate chemistry and increased interocean deep water exchange during last deglaciation. *Quat Sci Rev* 2014, **15:** 80-89.

43. Galbraith ED, Jaccard SL, Pedersen TF, Sigman DM, Haug GH, Cook M*, et al.* Carbon dioxide release from the North Pacific abyss during the last deglaciation. *Nature* 2007, **449:** 890-893.

44. Ronge TA, Tiedemann R, Lamy F, Köhler P, Alloway BV, De Pol-Holz R*, et al.* Radiocarbon constraints on the extent and evolution of the South Pacific glacial carbon pool. *Nat Commun* 2016, **7:** https://doi.org/10.1038/ncomms11487.

45. Gottschalk J, Vázquez Riveiros N, Waelbroeck C, Skinner LC, Michel E, Duplessy J-C*, et al.* Carbon isotope offsets between benthic foraminifer species of the genus Cibicides (Cibicidoides) in the glacial sub-Antarctic Atlantic. *Paleoceanogr* 2016, **31**(12)**:** 1583-1602.

46. Gottschalk J, Skinner LC, Lippold J, Vogel H, Frank N, Jaccard SL*, et al.* Biological and physical controls in the Southern Ocean on past millennial-scale atmospheric CO2 changes. *Nat Commun* 2016, **7:** https://doi.org/10.1038/ncomms11539.

47. Basak C, Fröllje H, Lamy F, Gersonde R, Benz V, Anderson RF*, et al.* Breakup of last glacial deep stratification in the South Pacific. *Science* 2018, **359**(6378)**:** 900-904.

48. Jacobel AW, McManus JF, Anderson RF, Winckler G. Repeated storage of respired carbon in the equatorial Pacific Ocean over the last three glacial cycles. *Nat Commun* 2017, **8**(1)**:** 10.1038/s41467-41017-01938-x.

49. Bereiter B, Eggleston S, Schmitt J, Nehrbass-Ahles C, Stocker TF, Fischer H*, et al.* Revision of the EPICA Dome C CO2 record from 800 to 600 kyr before present. *Geophysical Research Letters* 2015, **42**(2)**:** 542-549.

50. Schlitzer R. Ocean Data View. 2006, **http://odv.awi-bremerhaven.de**.

51. Barker S, Greaves M, Elderfield H. A study of cleaning procedures used for foraminiferal Mg/Ca paleothermometry. *Geochem Geophys Geosyst* 2003, **4**(9)**:** doi:10.1029/2003GC000559.

52. Yu JM, Elderfield H, Greaves M, Day J. Preferential dissolution of benthic foraminiferal calcite during laboratory reductive cleaning. *Geochem Geophys Geosyst* 2007, **8:** Q06016, doi:06010.01029/02006GC001571.

53. Yu JM, Day J, Greaves M, Elderfield H. Determination of multiple element/calcium ratios in foraminiferal calcite by quadrupole ICP-MS. *Geochem Geophys Geosyst* 2005, **6:** Q08P01, doi:10.1029/2005GC000964.

54. Feely RA, Sabine C, Lee K, Berelson WM, Kleypas J, Fabry VJ*, et al.* Impact of anthropogenic CO_2 on the $CaCO_3$ system in the oceans. *Science* 2004, **305:** 362-366.

55. Grant KM, Rohling EJ, Bar-Matthews M, Ayalon A, Medina-Elizalde M, Bronk Ramsey C*, et al.* Rapid coupling between ice volume and polar temperature over the past 150,000 years. *Nature* 2012, **491:** 744-747.

56. Mackensen A, Hubberten H-W, Bickert T, Fischer G, Fütterer DK. The $\delta^{13}C$ in benthic foraminiferal tests of *Fontbotia wuellerstorfi* (schwager) relative to the $\delta^{13}C$ of dissolved inorganic carbon in Souther Ocean deep water: Implications for glacial ocean circulation models. *Paleoceanogr* 1993, **8**(5)**:** 587-610.

57. Hodell DA, Venz KA, Charles CD, Ninnemann US. Pleistocene vertical carbon isotope and carbonate gradients in the South Atlantic sector of the Southern Ocean. *Geochem Geophys Geosyst* 2003, **4:** doi:10.1029/2002GC000367.

58. Curry WB, Oppo D. Glacial water mass geometry and the distribution of $\delta^{13}C$ of ΣCO_2 in the western Altantic Ocean. *Paleoceanogr* 2005, **20:** PA1017, doi:1010.1029/2004PA001021.

59. Lisiecki LE, Raymo ME. A Pliocene-Pleistocene stack of 57 globally distributed benthic $\delta^{18}O$ records. *Paleoceanogr* 2005, **20:** PA1003, doi:1010.1029/2004PA001071.

60. Ninnemann US, Charles CD. Changes in the mode of Southern Ocean circulation over the last glacial cycle revealed by foraminiferal stable isotopic variability. *Earth Planet Sci Lett* 2002, **201**(2)**:** 383-396.

Correspondence and requests for materials should be addressed to JY (jimin.yu@anu.edu.au).

Acknowledgments We thank Ping Wang for the long-time service with foraminifera shell picking in the lab. This work is supported by NSFC41676026, ARC Discovery Projects (DP140101393, DP190100894) and Future Fellowship (FT140100993) to JY, Future Fellowship (FT180100606) and Discovery (DP180100048) to LM, NSFC (41991322 and 41930864) to ZDJ, and Australian Laureate Fellowship (FL120100050) to EJR. The contribution of JFM was supported in part by the US-NSF. JY was in part supported by the "111" Project (BP0719030) when visiting PH Cai at Xiamen University.

Author contributions JY designed the project and wrote the paper. ZDJ/FZ managed shell picking. AMP/JFM arranged samples. AMP assisted seawater neodymium data compilation. XM plotted Fig. 2. All authors commented on the manuscript.

Competing interests. The authors declare no competing interests.

Supplementary information is available in the online version of the paper with inputs from all authors. Reprints and permissions information is available online at www.nature.com/reprints.

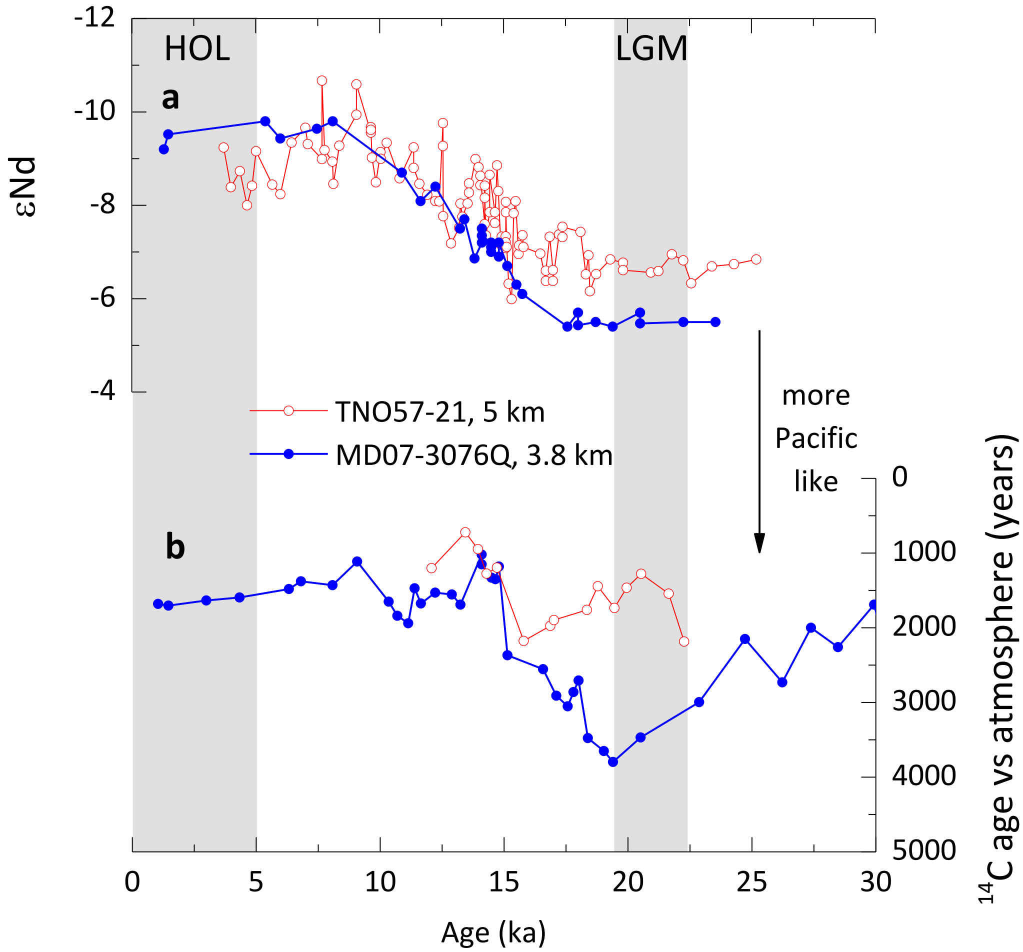

Fig. 1 | Comparison of εNd and ^{14}C ages at 3.8 and 5 km water depths in the South Atlantic Ocean. a, εNd. **b**, ^{14}C ages. Note that the shallower core MD07-3076Q had more Pacific-like εNd and ^{14}C-age signatures than the abyssal core TNO57-21 during the LGM. See Fig. 2 for core locations. Data are from refs [5,6,14,15].

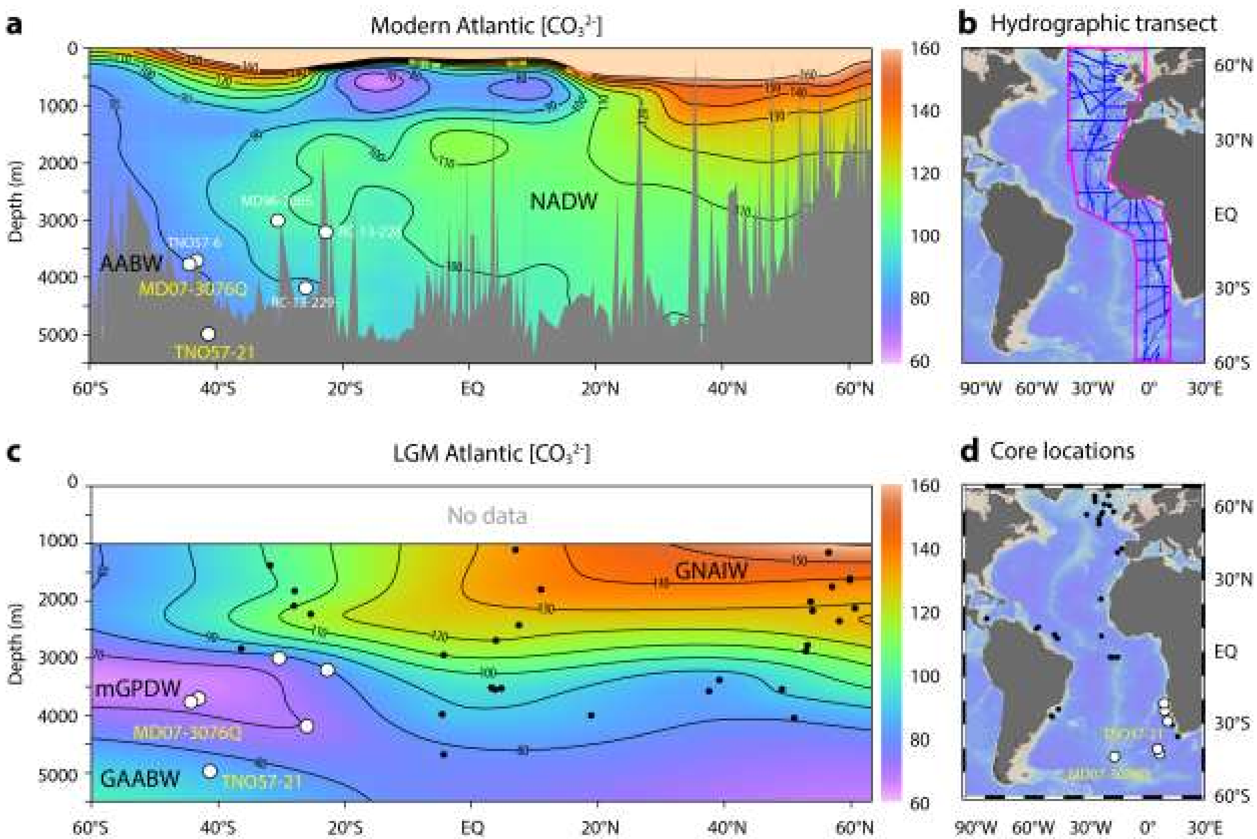

See a separate PDF file for a high-resolution figure.

Fig. 2 | Modern and LGM Atlantic meridional [CO_3^{2-}] transects. **a**, Modern [CO_3^{2-}] (unit: μmol/kg) transect for hydrographic sites shown in **b** compiled by the GLODAP dataset[11]. **c**, Reconstructed LGM [CO_3^{2-}] transect, using [CO_3^{2-}] reconstructions for all studied cores (dots and white filled circles shown in **c** and **d**). White filled circles shown in **a** and **c** denote locations of the five cores at 3-4 km and an abyssal core at ~5 km from the South Atlantic. Bright yellow labelling indicates locations of cores TNO57-21 and MD07-3076Q, whose long records are investigated (Fig. 4). NADW = North Atlantic Deep Water, AABW = Antarctic Bottom Water, GNAIW = Glacial North Atlantic Intermediate Water, GAABW = Glacial AABW, mGPDW = modified Glacial Pacific Deep Water. Maps are generated using Ocean Data View[50] (see Methods).

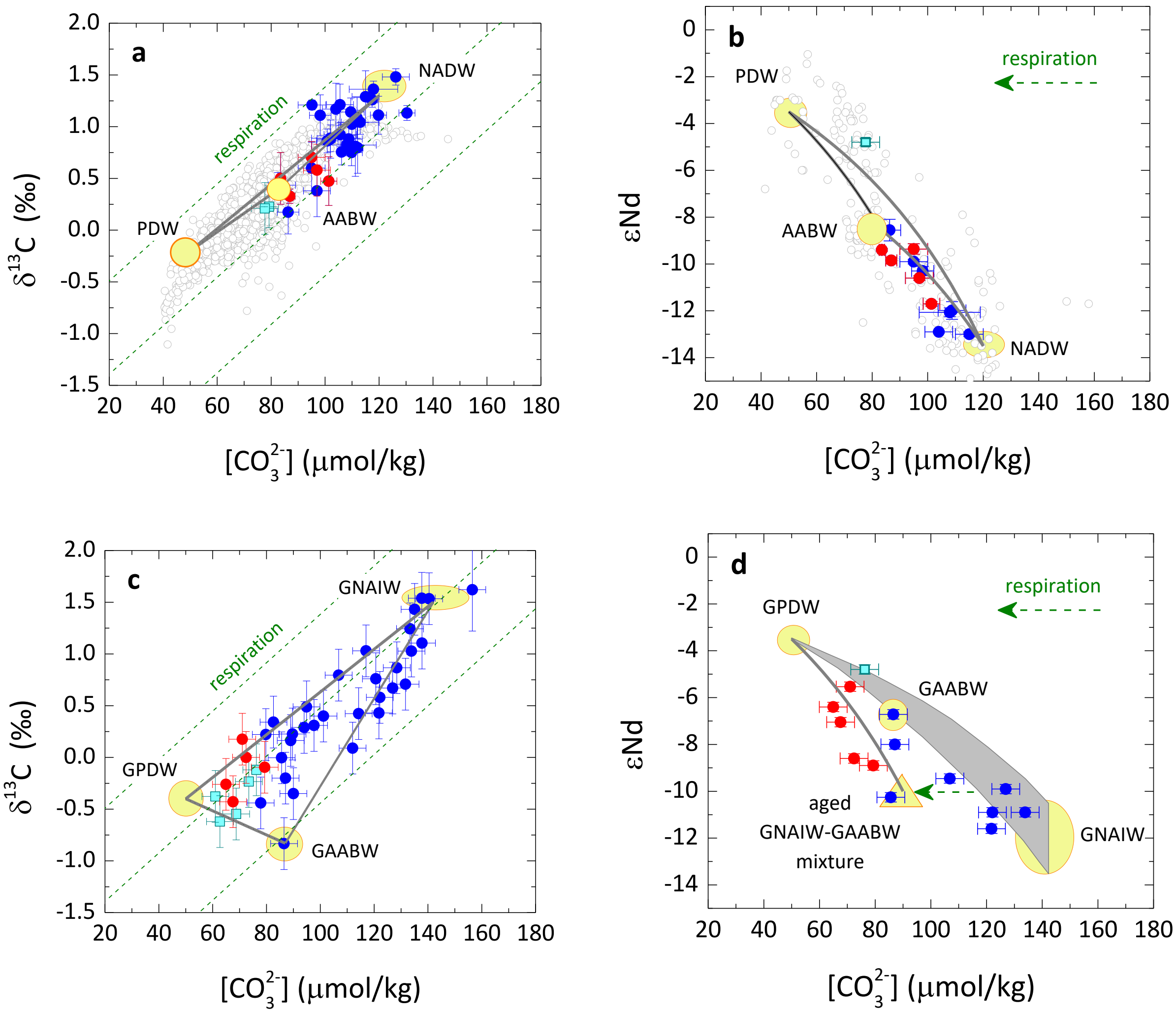
a
NADW
respiration
AABW
PDW
δ13C (‰)
[CO3 2-] (μmol/kg)
b
respiration
PDW
AABW
NADW
εNd
[CO3 2-] (μmol/kg)
c
GNAIW
respiration
GPDW
GAABW
δ13C (‰)
[CO3 2-] (μmol/kg)
d
respiration
GPDW
GAABW
aged
GNAIW-GAABW
mixture
GNAIW
εNd
[CO3 2-] (μmol/kg)

Fig. 3 | Paired $[CO_3^{2-}]$-$\delta^{13}C$-εNd. a, Holocene $\delta^{13}C$-$[CO_3^{2-}]$. **b**, Holocene εNd-$[CO_3^{2-}]$. **c**, LGM $\delta^{13}C$-$[CO_3^{2-}]$. **d**, LGM εNd-$[CO_3^{2-}]$. Red circles show sites at 3-4 km from the South Atlantic (Fig. 2), compared with other Atlantic locations (blue circles) and sites at 3-4 km from the equatorial Pacific Ocean (cyan squares). Grey circles show modern hydrographic data[11] (Supplementary Table 9). Large yellow circles/ovals represent endmember values (Supplementary Table 3). The yellow triangle in **d** denotes a hypothetical aged GNAIW-GAABW mixture, but also note other scenarios (Supplementary Fig. 5). Green dashed lines (**a**, **c**) represent the Redfield slope[23], while dashed arrows (**b**, **d**) indicate biological respiration effects. Grey lines/curves/shaded regions show conservative mixing of water masses. The mixing curvature for $\delta^{13}C$-$[CO_3^{2-}]$ is almost linear, but that for εNd-$[CO_3^{2-}]$ is much greater due to large endmember [Nd] contrasts (Supplementary Fig. 6). Due to biological respiration and uncertainties associated with endmember values including [Nd] and εNd, mixing trends should be treated as a guide for qualitative, not quantitative, estimates of mixing effects. Error bars: 1σ. See Methods for details.

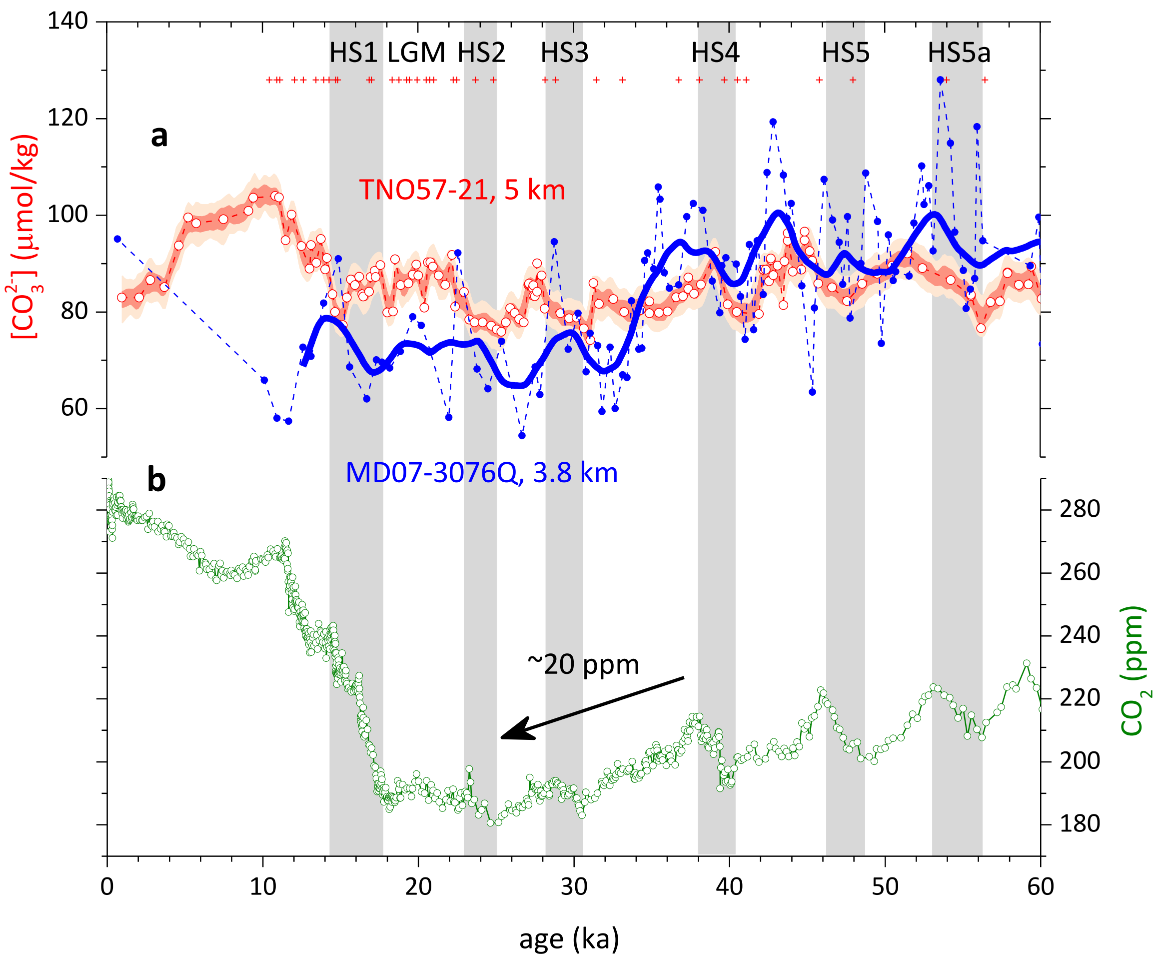

Fig. 4 | South Atlantic $[CO_3^{2-}]$ reconstructions at 3.8 and 5 km water depths compared with atmospheric CO_2 during the last 60 ka. **a**, Deep-water $[CO_3^{2-}]$ for TNO57-21 (0-27 ka: ref. [42]; 27-60 ka: this study) and MD07-3076Q[28]. Age models (crosses) are from ref. [27]. Dark and light red envelopes represent 1σ and 2σ uncertainties, respectively (Methods). Bold blue curve shows 3-kyr smoothing mean. **b**, Atmospheric CO_2[49]. The arrow represents the last ~20 ppm atmospheric CO_2 drawdown during the last glacial cycle which was coeval with the reversal of $[CO_3^{2-}]$ gradient between MD07-3076Q and TNO57-21. HS = Heinrich Stadial.

Methods

Samples and analytical methods. For the LGM Atlantic transect mapping (Fig. 2), we have measured (n = 19 cores) and compiled (n = 22 cores) benthic B/Ca for 41 sediment cores from the Atlantic and Pacific oceans. Age models are based on published chronologies (see Supplementary Table 1). For three cores, samples from <~8 ka are treated as the Holocene age (defined as 0-5 ka here), but exclusion of these samples do not affect our conclusion. For new samples analyzed in this study, sediments (~10-20 cm^3 from ~2 cm thickness each) were disaggregated in de-ionized water and wet sieved through 63 μm sieves. Except for ODP 1087 for which *C. mundulus* was used, we picked *C. wuellerstorfi* (generally ~10-20 tests for each sample) from the 250-500 μm size fraction. The shells were double checked under a microscope before crushing to ensure consistent shell morphology used for measurements. Following this careful screening the starting material for each sample was on average ~8-12 shells, which is equivalent to ~300-600 μg of carbonate. For benthic B/Ca analyses, foraminiferal shells were cleaned with the "Mg-cleaning" method[51,52]. Benthic B/Ca ratios were measured on an inductively-coupled plasma mass spectrometer (ICP-MS) using procedures outlined in ref. [53], with an analytical error better than ~5%. Regarding down-core analyses for TNO57-21, we have extended the benthic B/Ca record back to 60 ka, following the same approach given in ref. [42]. We have also measured benthic foraminifera stable isotopes for 4 cores, with analytical precision of ~0.08‰ for $\delta^{18}O$ and $\delta^{13}C$.

All new (n = 173 samples) and compiled (n = 260 samples) $[CO_3^{2-}]$ reconstructions together with paired benthic $\delta^{13}C$ and εNd are provided in the Supplementary Tables 1-11.

Deep water [CO_3^{2-}] reconstructions. Deep-water [CO_3^{2-}] values are reconstructed using benthic B/Ca (refs [12,17]) from $[CO_3^{2-}]_{downcore} = [CO_3^{2-}]_{PI} + \Delta B/Ca_{downcore-coretop}/k$, where $[CO_3^{2-}]_{PI}$ is the preindustrial (PI) deep-water [CO_3^{2-}] value estimated from the GLODAP dataset[11], $\Delta B/Ca_{downcore-coretop}$ represents the deviation of B/Ca of down-core samples from the core-top value, and k is the B/Ca-[CO_3^{2-}] sensitivity of *C. wuellerstorfi* (1.14 μmol/mol per μmol/kg) or *C. mundulus* (0.69 μmol/mol per μmol/kg)[17]. To calculate $[CO_3^{2-}]_{PI}$, we have removed anthropogenic influences on DIC after ref. [54]. We use a reconstruction uncertainty of 5 μmol/kg (1σ) in [CO_3^{2-}] based on global core-top calibration samples[17].

Mapping of LGM [CO_3^{2-}] data. Given limited number reconstructions that is almost always the case for palaeoceanographic studies, all cores are projected onto a single, arbitrary latitudinal-water depth plane for the LGM plotting (Fig. 2c), an approach widely used for mapping of other proxies like εNd and $\delta^{13}C$[1,3,19]. Ocean Data View is employed to generate Fig. 2c using the average [CO_3^{2-}] values (Supplementary Table 2). Contours are generated using the DIVA gridding with X and Y scale-length values of 110 and 104, respectively. Quality limit is set to 7. Linear mapping option is used for color mapping.

Modern seawater [CO_3^{2-}]-$\delta^{13}C$-εNd data. In Fig. 3a, modern seawater [CO_3^{2-}]-$\delta^{13}C$ data are from the GLODAP dataset[11]. Seawater εNd data shown in Fig. 3b are compiled from the literature for water depths from > 1 km, while their corresponding seawater [CO_3^{2-}] are estimated using the GLODAP dataset[11], not measured along with εNd analyses. Associated data are provided in Supplementary Tables 9-10.

Water mass mixing. The chemical and isotopic signatures of mixtures of two waters are calculated by

$$[X]_M = [X]_A \times f_A + [X]_B \times (1 - f_A) \quad (1)$$

$$\delta_M \times [X]_M = \delta_A \times [X]_A \times f_A + \delta_B \times [X]_B \times (1 - f_A) \quad (2)$$

where [X] and δ are, respectively, endmember concentrations and chemical signatures of tracers (elements or compounds) of interest, subscripts A, B, and M represent water mass A, B and their mixture, respectively, and f_A is the fraction of water mass A in the mixture. Here, X denotes C, Nd, or DIC, while δ represents $\delta^{13}C$, εNd, or $[CO_3^{2-}]$. Thus, we can obtain

$$\delta_M = (\delta_A \times [X]_A \times f_A + \delta_B \times [X]_B \times (1 - f_A)) \div ([X]_A \times f_A + [X]_B \times (1 - f_A)) \quad (3)$$

The endmember values used to calculate "reference" mixing curves shown in Fig. 3 are given in Supplementary Table 3. The endmember [Nd] values are assumed to be unchanged between modern water masses and their LGM counterparts, but it is important to note that past seawater [Nd] remains poorly constrained.

For the hypothetical aged GNAIW-GAABW mixture shown in Fig. 3d, we use [Nd] = 22 pmol/kg, εNd = -10, $[CO_3^{2-}]$ = 90 μmol/kg, and DIC = 2300 μmol/kg. More scenarios to explain the LGM εNd-$[CO_3^{2-}]$ data are given in Supplementary Fig. 5.

The mixing curvature depends on the relative difference between $[X]_A$ and $[X]_B$. For the $\delta^{13}C$-$[CO_3^{2-}]$ system, the mixing curvature is insensitive to endmember DIC changes because water-mass DIC contrasts are small (<10%) and DIC-weighing applies to both $[CO_3^{2-}]$ and $\delta^{13}C$. By contrast, the curvature is greater for the εNd-$[CO_3^{2-}]$ system, driven by the large [Nd] difference (up to ~50%-100%) between water masses (Fig. 3). A various sensitivity test is given in Supplementary Fig. 6, by changing endmember [Nd] and DIC values.

Note that we assume tracers remain conservative, with no addition or removal of ingredients, during mixing of water masses. This is likely an oversimplification. Thus, mixing lines/regions shown (Fig. 3; Supplementary Fig. 5) should be treated as a guide to aid interpretation of data instead of using them for accurate quantification of mixing ratios. Importantly, insufficient knowledge about [Nd] and the potentially large endmember εNd range for GNAIW (Fig. 3) preclude estimates of exact mixing scenarios for the LGM, although the data do provide useful clues about mixing schemes in a qualitative sense.

Statistical analyses. For TNO57-21 downcore record, uncertainties associated with $[CO_3^{2-}]$ were evaluated using a Monte-Carlo approach[55]. Errors associated with the chronology (x-axis) and $[CO_3^{2-}]$ reconstructions (y-axis) are considered during error propagation. Age errors are estimated following ref. [27]. Error for each $[CO_3^{2-}]$ reconstruction is 5 μmol/kg. All data points were sampled separately and randomly 5,000 times within their chronological and $[CO_3^{2-}]$ uncertainties and each iteration was then interpolated linearly. At each time step, the probability maximum and data distribution uncertainties of the 5,000 iterations were assessed. Fig. 4a shows ±1σ (dark red envelopes; 16th-84th percentile) and ±2σ (light red; 2.5th-97.5th percentile) probability intervals for the data distributions, including chronological and proxy uncertainties.

GAABW $\delta^{13}C$ endmember. The LGM benthic $\delta^{13}C$ in core TNO57-21 has long been used as the GAABW $\delta^{13}C$ endmember value[1,2,19]. However, the extent to which the observed low benthic $\delta^{13}C$ (~-0.8‰) reflects seawater $\delta^{13}C$ during the LGM is a matter of long-lasting debate, and no consensus has been reached to date[45,56,57]. For scenario shown in Supplementary Fig. 8a, glacial benthic foraminiferal $\delta^{13}C$ could be biased to lower values relative to deep-water $\delta^{13}C$, if epifaunal benthic species (generally thought to live above the sediment-deep water boundary) somehow lived in pore waters or phytodetritus layers during the LGM[56]. In this scenario, reconstructions using benthic foraminiferal shells would reflect pore-water/"fluffy"-layer chemistry, instead of deep-water chemistry. Deep-water $\delta^{13}C$ and $[CO_3^{2-}]$ values could be inferred from TNO57-21 data and the Redfield slope (pink arrow)[23]. For illustration purpose, the yellow circle represents only one possibility for GAABW $\delta^{13}C$ and $[CO_3^{2-}]$ values, because the exact magnitude of chemical offset between deep-waters and pore-waters/fluffy-layers remains unknown for the LGM. Nevertheless, the inferred higher $\delta^{13}C$ and $[CO_3^{2-}]$ values for GAABW would still require mixing of GPDW to explain low-$[CO_3^{2-}]$ signature observed in the 3-4 km of the South Atlantic.

For scenario shown in Supplementary Fig. 8b, benthic $\delta^{13}C$ is corrected by +0.76‰ (ref. [45]) to account for pore water influences, assuming that *Cibicidoides* (used for $\delta^{13}C$ analyses) lived in pore waters. No correction is applied to $[CO_3^{2-}]$ reconstructions, assuming that *C. wuellerstorfi* (used for B/Ca measurements) lived in deep-waters. In this scenario, the low-$[CO_3^{2-}]$ and low-$\delta^{13}C$

observed in 5 cores at 3-4 km from the South Atlantic (red circles) could be explained by aging of GAABW-GNAIW mixtures. This may alleviate, but does not exclude, the need for GPDW involvement. However, the applicability of +0.76‰ correction (obtained from other cores)[45] is yet to be justified for core TNO57-21. Also, this scenario would leave many data points (blue shaded area) plotting blow the mixing trends, unexplained.

Both scenarios are speculative and additional work is needed to approve/disapprove these possibilities. Neither scenarios exclude the GPDW involvement as we suggest in this study. At present, existing evidence is insufficient to justify the reliability of these scenarios, leaving them highly speculative. Thus, we continue to use ***measured*** $\delta^{13}C$ values of ~-0.8‰ as the GAABW endmember, following the previous work[1,2,4,19,58]. It is important to emphasize that even considering scenarios for higher GAABW $\delta^{13}C$, our conclusion of GPDW expansion remains unchanged: a greater GPDW penetration into the deep South Atlantic is warranted to explain more radiogenic εNd observed at 3-4 km than at abyssal depths (~5 km; TNO57-21) (Fig. 1, 3d).

Data availability. All data presented in this study are provided in the Supplementary Information.

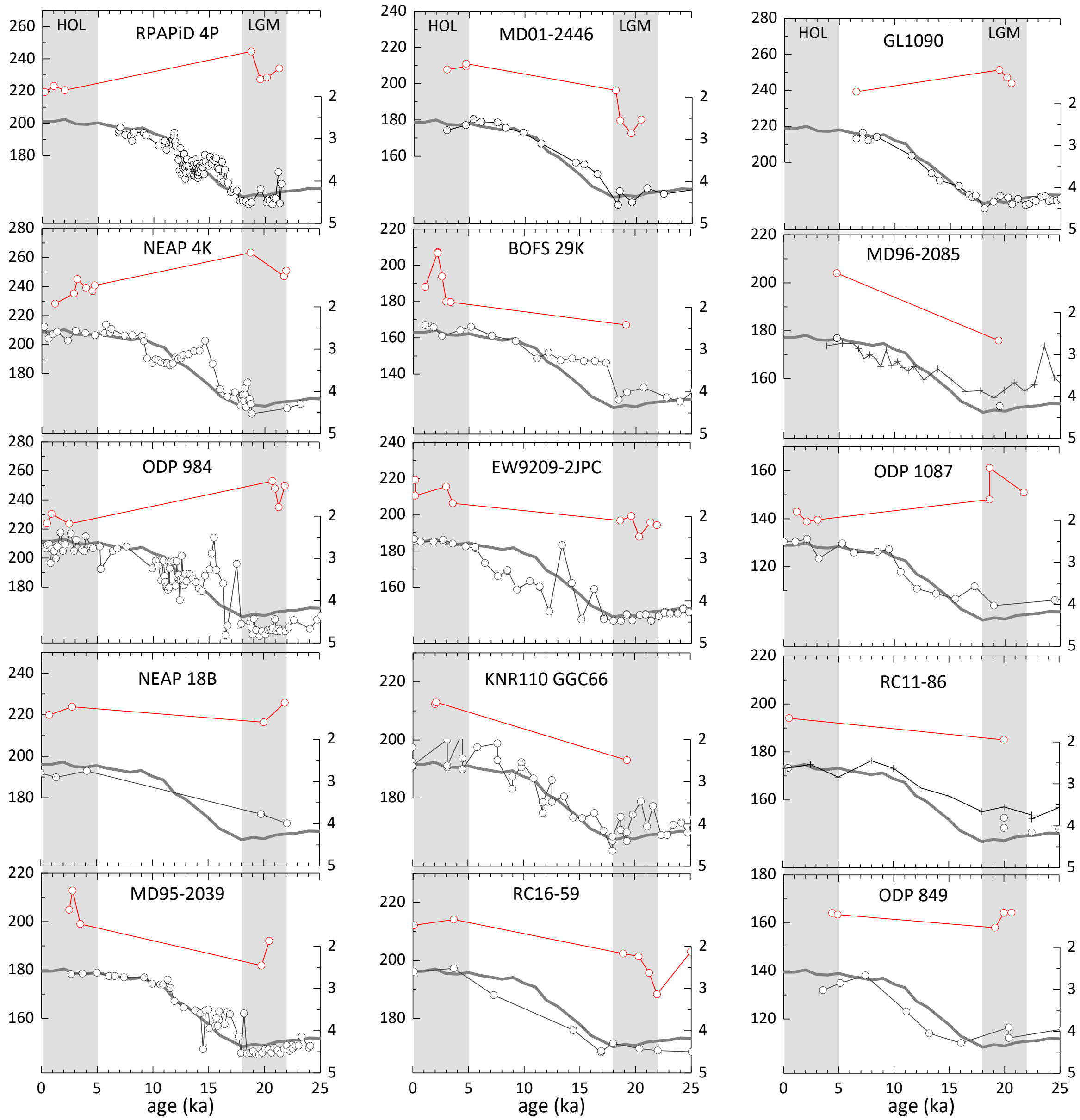

Extended Data Fig. 1 | New benthic B/Ca (red circles; unit: µmol/mol) against benthic δ^{18}O (grey circles; unit: ‰) and the LR04 record[59] (bold grey lines). For MD96-2085 and RC11-86, *G. inflata* and *G. sacculifer* δ^{18}O (crosses) are shown, after adjusted by +1.8‰ and +3‰, respectively. All benthic B/Ca shown are from this study. References for age models and δ^{18}O are given in Supplementary Table 1.

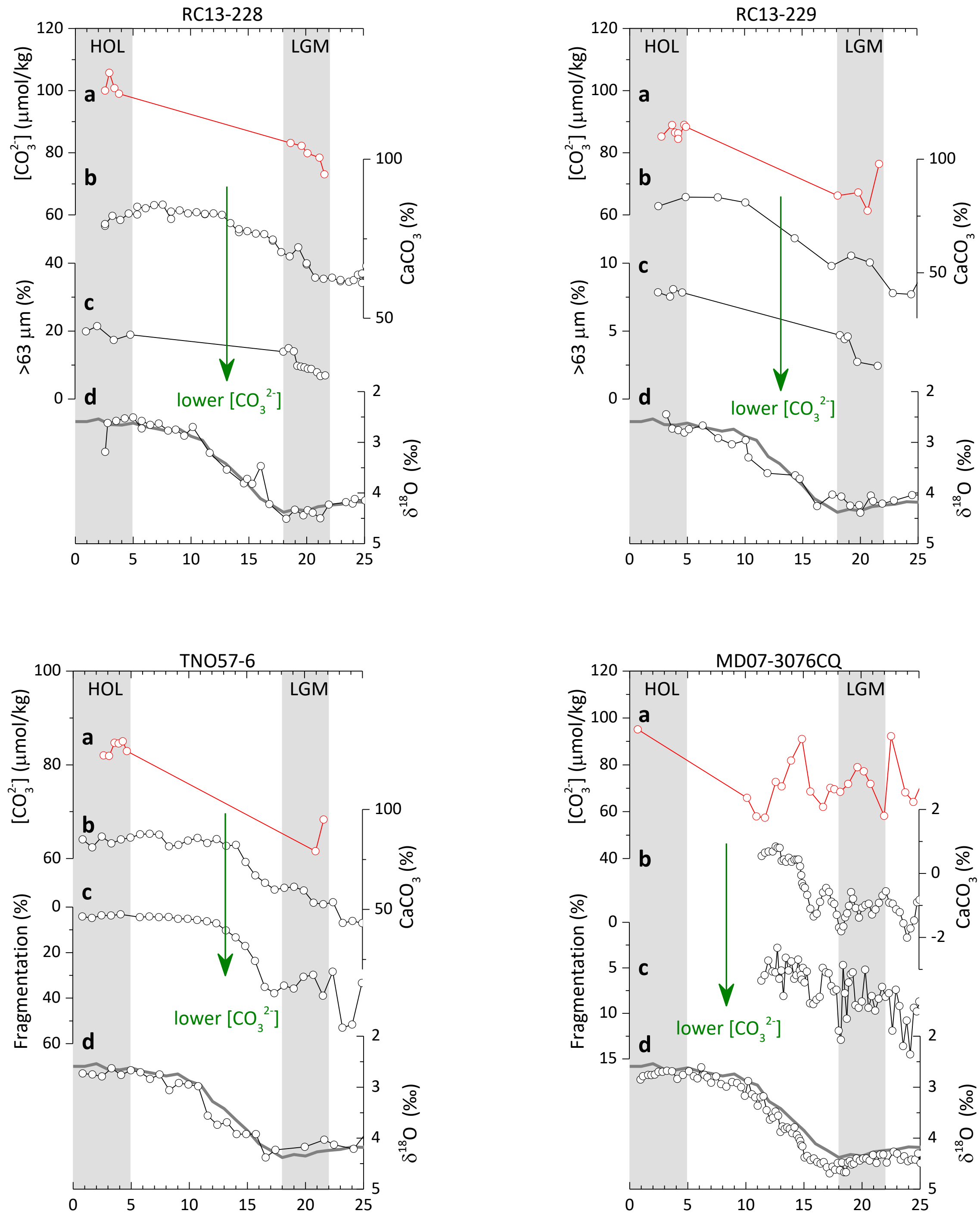

Extended Data Fig. 2 | New and published deep-water [CO_3^{2-}] using benthic B/Ca along with qualitative proxies for 3-4 km cores from the South Atlantic. For RC13-228, RC13-229, and TNO57-6, [CO_3^{2-}] are from this study, and %$CaCO_3$, >63 µm, and fragmentation are from ref. [26]. MD07-3076 data are from ref. [28]. Age models and $\delta^{18}O$ references are given in Supplementary Table 1. All cores show lower deep-water [CO_3^{2-}] during the LGM than the Holocene.

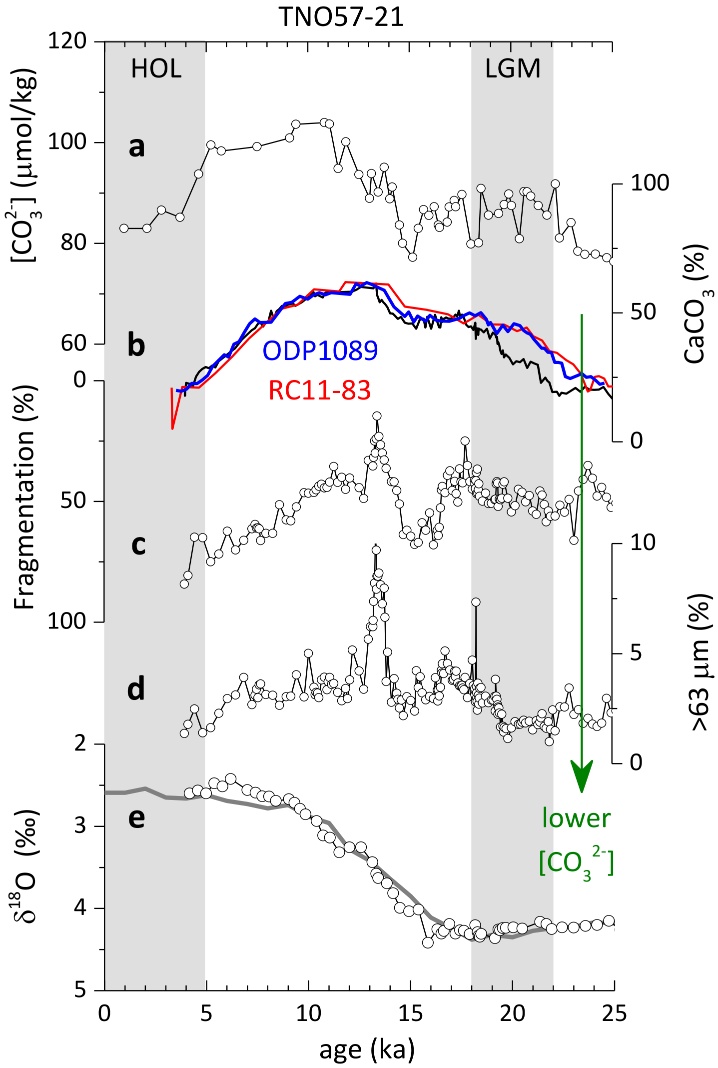

Extended Data Fig. 3 | Deep-water [CO_3^{2-}] based on benthic B/Ca along with qualitative [CO_3^{2-}] proxies in core TNO57-21 from the abyssal depth (~5 km) in the South Atlantic. Also shown are %$CaCO_3$ for another two abyssal cores RC11-83 (41.6°S, 9.8°E, 4718m) and ODP 1089 (40.9°S, 9.9°E, 4621m). Data are from refs [15,42,60]. All cores suggest slightly higher [CO_3^{2-}] at ~5 km in the South Atlantic during the LGM than the Holocene.

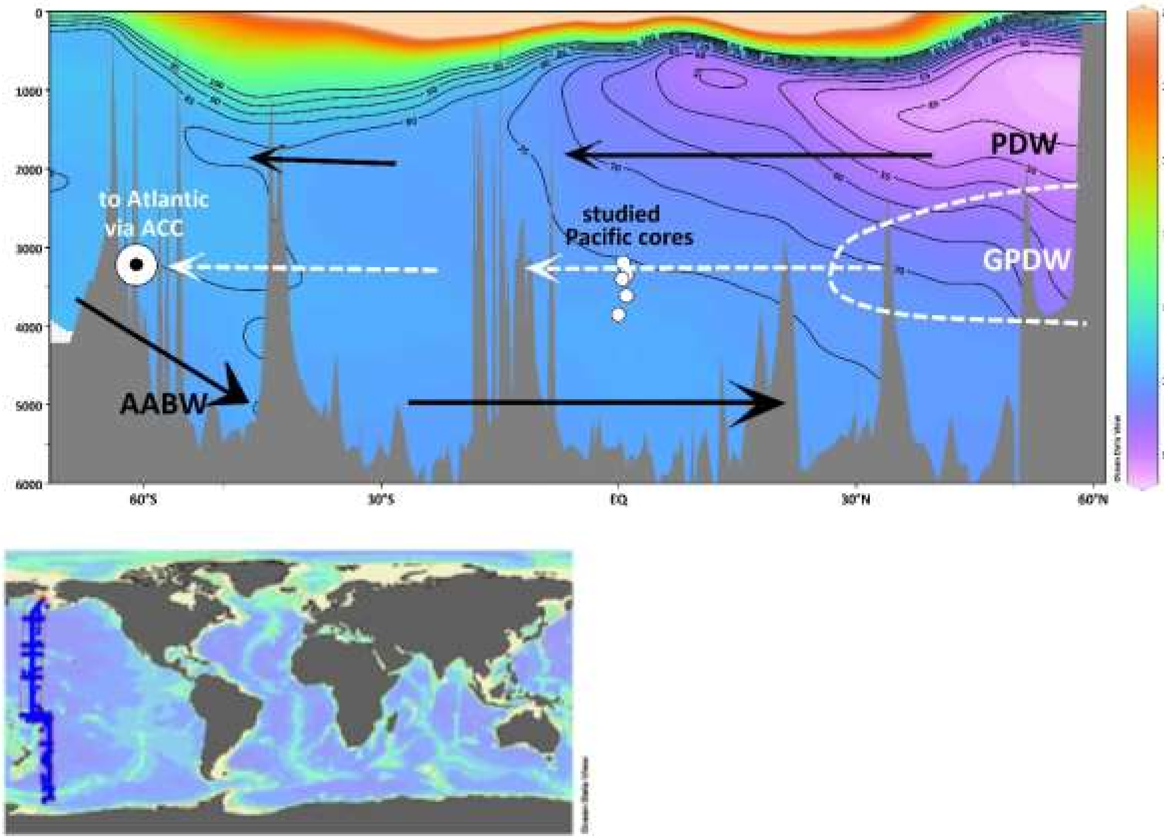

Extended Data Fig. 4 | Meridional Pacific Ocean [CO_3^{2-}] distribution. a, [CO_3^{2-}] transect. **b**, hydrographic sites[11] used to generate **a**. Today, the core of PDW is located at ~1-2 km in the polar North Pacific with a [CO_3^{2-}] of ~50 µmol/kg. The low [CO_3^{2-}] signature can be traced in the Southern Ocean (~50°S) due to the southward transport (southward black arrows) of PDW at ~1-2 km[33]. During the LGM, the core of GPDW is thought to deepen to ~3 km (dashed half circle)[34]. Our study suggests that the southward transport (dashed arrows) of GPDW was more extensive. By the time when GPDW was transported to the Pacific sector of the Southern Ocean, its signals would be transported via ACC (circle with an inner dot; transport out of the page) to the South Atlantic Ocean. White circles indicate cores at 3-4 km from the equatorial Pacific Ocean shown in Fig. 3. These cores show lower [CO_3^{2-}] than the abyssal South Atlantic waters (TNO57-21), indicating that GPDW likely had lower [CO_3^{2-}] than GAABW.

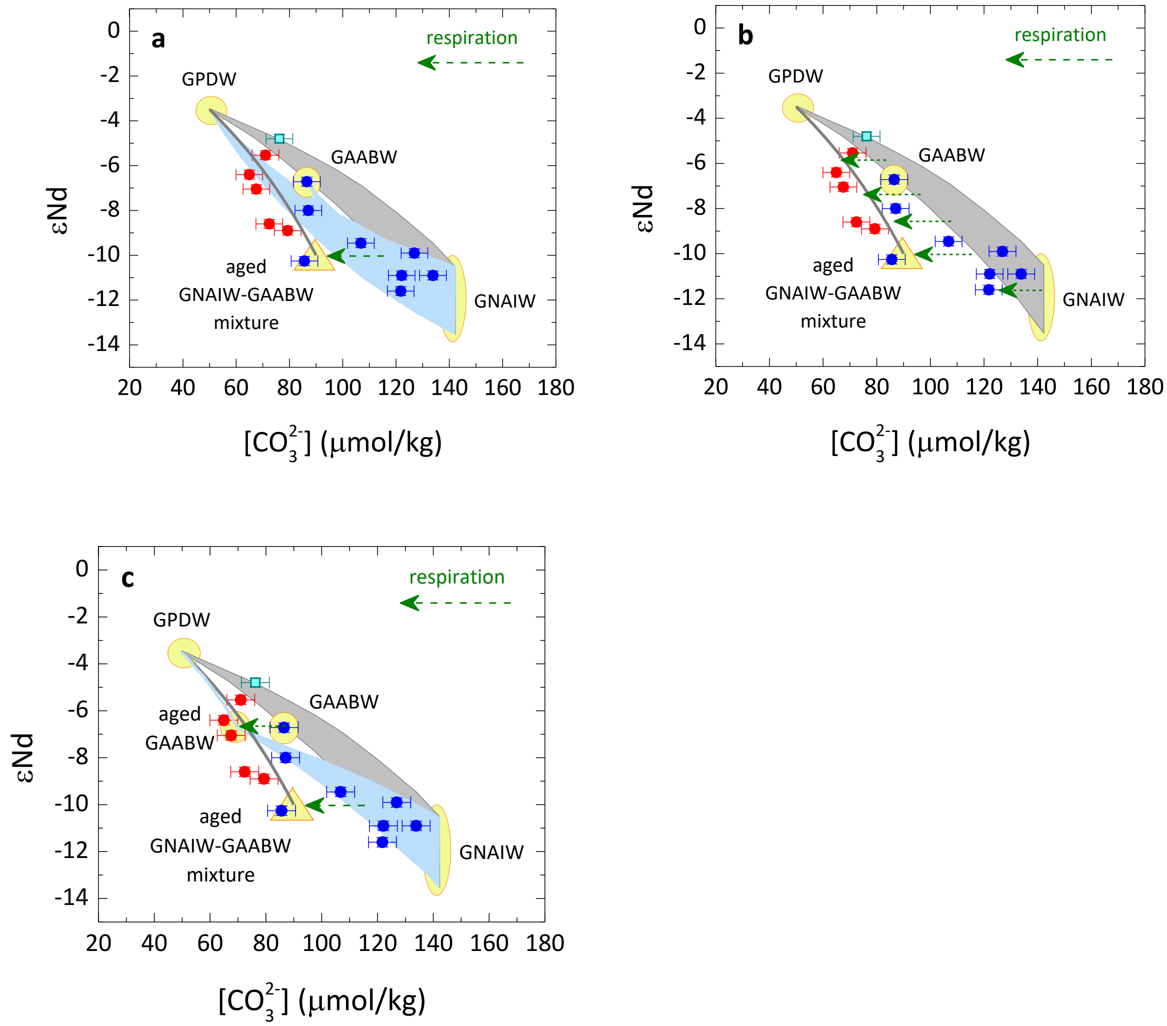

Extended Data Fig. 5 | Alternative scenarios that may contribute to interpretation of the LGM data. a, as Fig. 3d, but only triple [Nd] of GNAIW. New mixing trend is shown by the blue region. **b**, as Fig. 3d, but only invoke various degrees of biological respiration (dashed horizontal arrows) associated with GPDW-GAABW-GNAIW mixtures. **c**, as Fig. 3d, but mixing (blue region) with an aged and hence lower [CO_3^{2-}] (70 μmol/kg) GAABW. **Note that** these are just some examples that can potentially contribute to explaining the LGM data, and should not be treated as exhaustive. At present, uncertainties (e.g., large endmember εNd ranges and largely unconstrained [Nd]) preclude quantification of mixing ratios and respiration effects and their relative importance. Nevertheless, the more radiogenic εNd at 3.8 km (Fig. 1) would require mixing with GPDW.

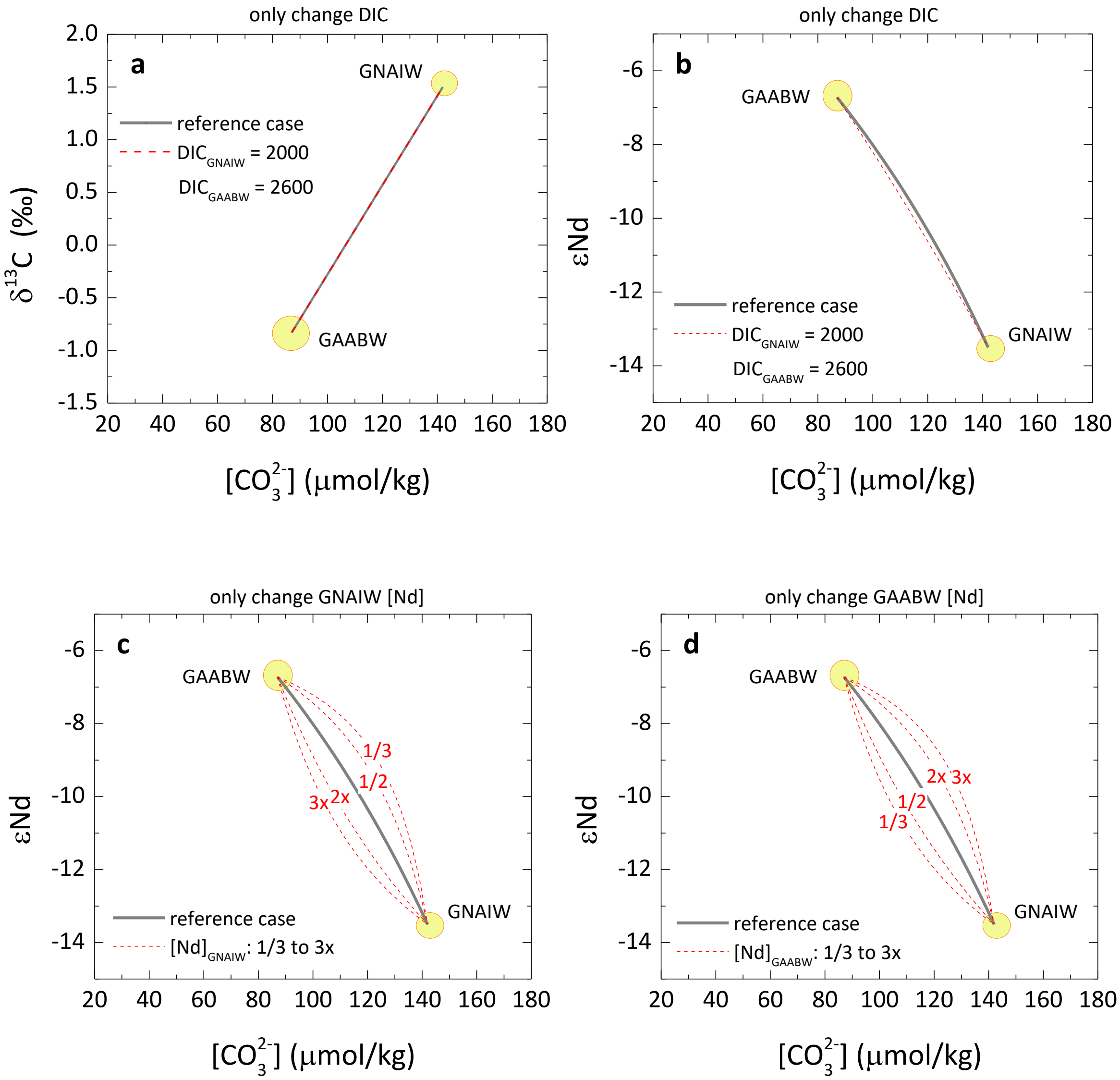

Extended Data Fig. 6 | Mixing curvature to water-mass endmember DIC and Nd contents. Effect of endmember DIC changes on (**a**) $\delta^{13}C$-[CO_3^{2-}] and (**b**) εNd-[CO_3^{2-}]. Relative to the reference cases (grey lines), DIC_{GNAIW} and DIC_{GAABW} are decreased and increased by 200 μmol/kg, respectively, to intentionally enlarge the DIC contrast between water masses. Effect of endmember [Nd] changes on (**c**) $\delta^{13}C$-[CO_3^{2-}] and (**d**) εNd-[CO_3^{2-}]. Endmember [Nd] are varied from 1/3 to 3× of the reference value for (**c**) GNAIW and (**d**) GAABW. To simplify the view, only GNIAW and GAABW are shown, and GNIAW εNd is only considered at -13.5. This figure suggests that mixing curvature is insensitive to endmember DIC changes, but sensitive to [Nd] changes.

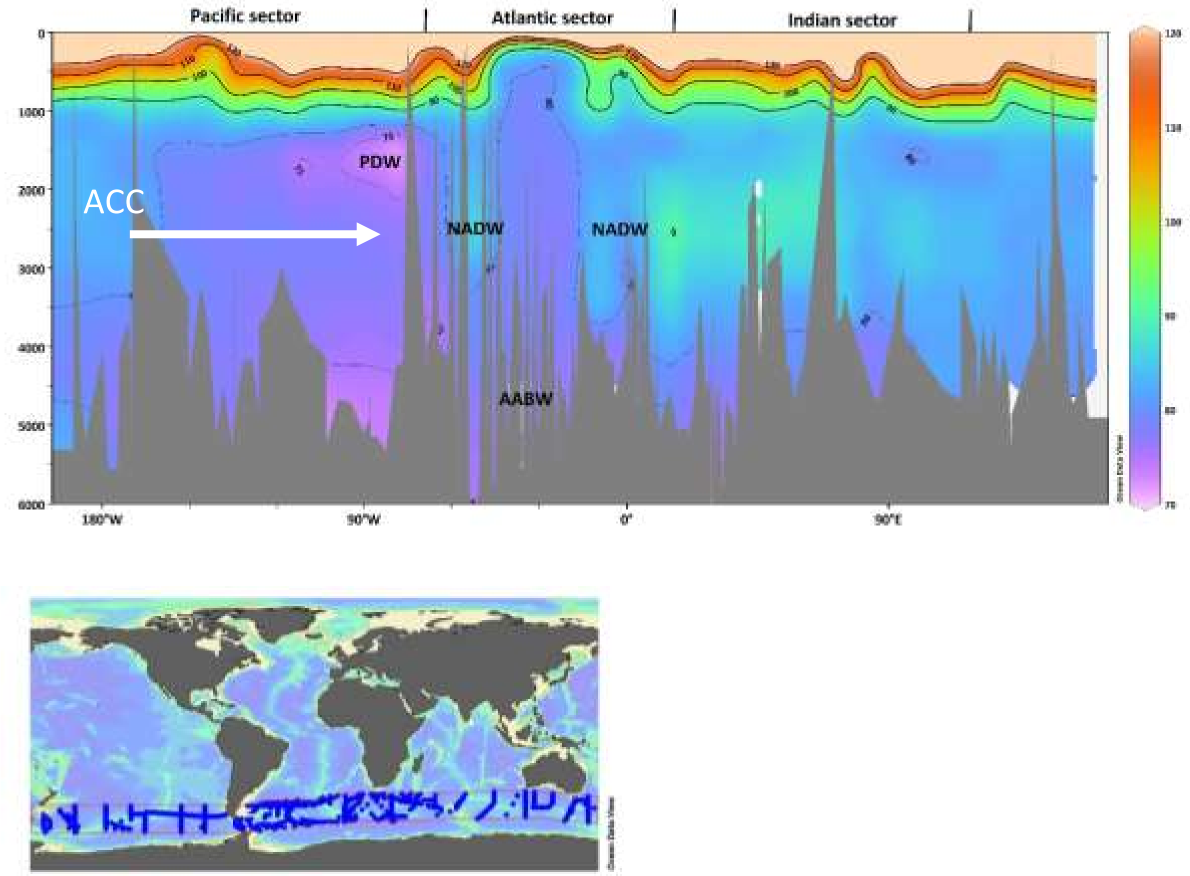

Extended Data Fig. 7 | Zonal distribution of $[CO_3^{2-}]$ in the Southern Ocean. a, Seawater $[CO_3^{2-}]$ for three sectors of the Southern Ocean. **b**, Hydrographic sites (~50-60°S)[11] used to generate **a**. In today's Southern Ocean, $[CO_3^{2-}]$ is not zonally homogeneous. Instead, the low-$[CO_3^{2-}]$ PDW signature is seen in relatively restricted regions at ~1-2 km in the Pacific sector of the Southern Ocean. Via ACC, this signal would be transported to other sectors including the South Atlantic, although its influence is not very clearly seen due to strong vertical mixing that tends to erode any signal anomalies. Our study suggests that the influence of GDPW was more extensive and deeper (~3-4 km) in the Southern Ocean during the LGM. GPDW influence is recorded by $[CO_3^{2-}]$ and other proxies (e.g., εNd and ^{14}C) from the deep South Atlantic.

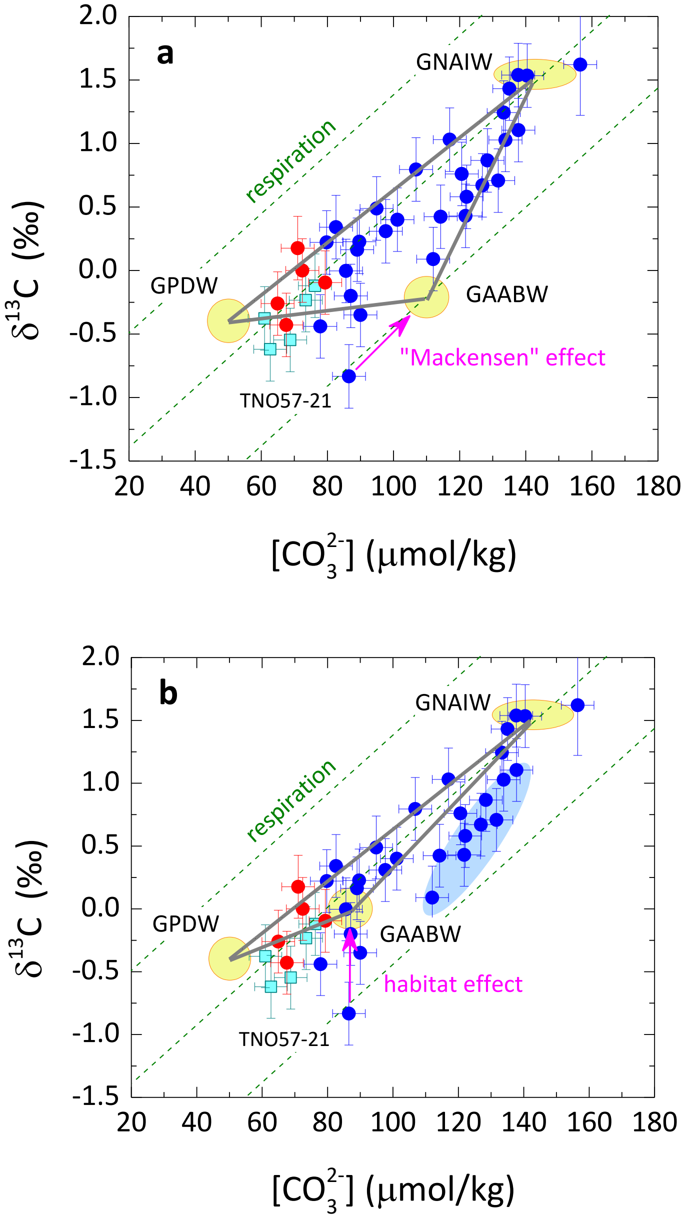

Extended Data Fig. 8 | Scenarios for different GAABW $\delta^{13}C$ values. a, "Mackensen" effects that would affect both deep-water $\delta^{13}C$ and $[CO_3^{2-}]$. **b**, Habitat change that only affects deep-water $\delta^{13}C$. See "GAABW $\delta^{13}C$ endmember" in Methods for details.

	$[CO_3^{2-}]$	DIC	ref	$\delta^{13}C$	ref	εNd	[Nd]	ref
	μmol/kg	μmol/kg		‰			pmol/kg	
NADW	120	2140	[23]	1.3	[3]	-13.5	17.5	[3]
AABW	83	2250	[23]	0.4	[1,58]	-8.5	25.1	[3]
PDW	50	2380	[11]	-0.2	[11,34]	-3.5	35	[3]
GNAIW	142 ± 8	*2200*#	*	1.5	[1,58]	-13.5 to -10.5	17.5	εNd: [3,29]; [Nd]: [3]
GAABW	87 ± 4	*2400*#	*	-0.83	[58]	-6.72	25.1	εNd: *; [Nd]: [3]
GPDW	50	*2600*#	[37,38]	-0.4	[34,36]	-3.5	35	εNd: [35]; [Nd]: [3]

Extended Data Fig. 9 | Endmembers for modern and LGM water masses. #: Italic numbers are assumed values, and using other values would have little effect on mixing lines shown in Fig. 3, due to insensitivity of mixing curvature to DIC values (see Extended Data Fig. 6). *: This study; see Supplementary Tables 1 and 2 for cores used to define associated endmembers.

				Holocene		**LGM**		**LGM-HOL diff**
Core	Lat.	Long.	water depth	[CO_3^{2-}]	sd	[CO_3^{2-}]	sd	[CO_3^{2-}]
	°N	°W	m	μmol/kg		μmol/kg		μmol/kg
BOFS 8K	53	22	4045	102	7	80	4	-22
BOFS 5K	51	22	3547	110	4	95	5	-15
MD95-2039	41	10	3381	106	6	89	6	-16
MD01-2446	39	13	3576	106	1	83	9	-24
BOFS 29K	20	21	4000	108	11	86	5	-22
EW9209-2JPC	6	44	3528	106	5	90	4	-16
KNR110 GGC66	5	43	3550	111	1	94	5	-17
RC16-59	4	43	3520	112	1	98	6	-14
GeoB1118	-4	16	4671	84	5	78	5	-6
RC13-228	-22	-11	3204	101	3	79	4	-22
RC13-229	-26	-11	4191	87	2	68	6	-19
MD96-2085	-30	-13	3001	97	5	72	5	-25
TNO57-21	-41	-8	4981	86	4	87	4	0
TNO57-6	-43	-9	3702	83	1	65	5	-19
MD07-3076CQ	-44	14	3770	95	5	71	4	-24
						Average:		**-17**
						sd:		**7**

Extended Data Fig. 10 | LGM-Holocene [CO_3^{2-}] difference for cores from >3 km in the Atlantic. sd: standard deviation.